Structure of Hydrous Ruthenium Oxides: Implications for Charge Storage

David A. McKeown,[†] Patrick L. Hagans,[‡] Linda P. L. Carette,[§] Andrea E. Russell,[§] Karen E. Swider,[‡] and Debra R. Rolison*[,‡]

Surface Chemistry Branch, 6170, Naval Research Laboratory, Washington, D.C. 20375, Vitreous State Laboratory, Catholic University of America, 620 Michigan Avenue, N.E., Washington, D.C. 20069, and Department of Chemistry, University of Southampton, Highfield, Southampton SO17 1BJ, United Kingdom

Received: January 7, 1999

Hydrous ruthenium oxide ($RuO_2 \cdot xH_2O$ or RuO_xH_y) is a mixed electron−proton conductor with a specific capacitance as high as 720 F/g/proton, making it a candidate material for energy storage. The correlation between the structure and properties of $RuO_2 \cdot xH_2O$ materials is not well understood due to their amorphous nature and compositional variability. In this study, ruthenium oxides with the compositions $RuO_2 \cdot 2.32H_2O$, $RuO_2 \cdot 0.29H_2O$, and anhydrous RuO_2 are characterized using thermogravimetric analysis (TGA), X-ray diffraction (XRD), and X-ray absorption near-edge structure (XANES) and extended X-ray fine structure (EXAFS) analyses. XANES cannot be used to distinguish between Ru(III) and Ru(IV) in the hydrous oxides, but the EXAFS analyses show large differences in the short-range structures of the materials. Whereas anhydrous RuO_2 has the rutile structure comprising chains of RuO_6 octahedra linked in three dimensions, the structure of $RuO_2 \cdot 0.29H_2O$ is rutile-like at the RuO_6 core, but less connected and progressively disordered beyond the RuO_6 core. The structure of $RuO_2 \cdot 2.32H_2O$ is composed of chains of disordered RuO_6 octahedra that exhibit no chain-to-chain linking or three-dimensional order. Although the local structures of $RuO_2 \cdot 0.29H_2O$ and $RuO_2 \cdot 2.32H_2O$ markedly differ, their specific capacitances are large and essentially equivalent, so nonunique local structures can balance effective electron transport (along dioxo bridges) with the effective proton transport (through structural water) necessary for charge storage.

Introduction

Hydrous ruthenium dioxide, $RuO_2 \cdot xH_2O$ or RuO_xH_y, exhibits mixed electron−proton conductivity,[1] unlike its anhydrous, crystalline parent rutile RuO_2, which is a metallic conductor.[2] $RuO_2 \cdot xH_2O$ has important technological applications and opportunities in electrocatalysis and charge storage. The active surface of the dimensionally stable anodes (DSAs) used to electrolyze brine to chlorine contains hydrated and defective RuO_2.[3−6] The $RuO_2 \cdot xH_2O$ content of the 50:50 at. % Pt−Ru black catalysts used in direct methanol fuel cells (DMFCs) correlates to their activity for methanol electrooxidation.[7−10] Various other catalytic aspects of hydrous ruthenium oxide have been documented in the literature.[11,12] $RuO_2 \cdot xH_2O$ ($x = 0.5$) is also under development as a pseudocapacitor because of its high specific capacitance (720 F/g/proton) resulting from its ability to transport and store both electrons and protons.[13,14] In addition, the mixed electron−proton conductivity observed for $RuO_2 + TiO_2$ mixed-phase aerogels is attributed to the presence of hydrous ruthenium oxide in this nanoscale mesoporous material.[1,15,16]

Despite the technological importance of $RuO_2 \cdot xH_2O$, this material has not been well characterized due to its structural disorder and variable chemistry, especially with respect to the oxidation state of Ru and its structural water or −OH content. The crystalline Ru(IV) oxide, RuO_2, has been thoroughly characterized and can be used as a reference material for the hydrous samples. RuO_2 has the rutile structure and is composed of RuO_6 octahedra, having four oxygen ions at 1.984 Å and two axial oxygen ions at 1.942 Å from the Ru^{4+} (Figure 1).[6,17] The octahedra are linked in chains along the *c* axis of the crystal structure by sharing two oxygen ions with each of two neighboring octahedra. The Ru−Ru distance of neighboring octahedra along these chains is 3.107 Å. Each octahedral chain links to four other neighboring chains by sharing oxygen ions to form a three-dimensional network, creating eight Ru−Ru distances at 3.535 Å.[17]

In this study, RuO_2 and two $RuO_2 \cdot xH_2O$ materials having different water contents are characterized using thermogravimetric analysis (TGA), X-ray diffraction (XRD), and X-ray absorption spectroscopy (XAS). Because the $RuO_2 \cdot xH_2O$ materials are amorphous or poorly crystalline, their structure is best elucidated from analysis of the extended X-ray absorption fine structure (EXAFS). The EXAFS of the $RuO_2 \cdot xH_2O$ materials and of anhydrous RuO_2 is compared to the calculated EXAFS for the rutile RuO_2 structure. The results from the EXAFS analyses and the associated structural interpretations suggest that the local structures of hydrous ruthenium oxides influence some of their electrochemical properties, particularly those involving charge storage.

Experimental Procedures

Chemicals and Determination of their Physical Properties. $RuO_2 \cdot xH_2O$ and RuO_2 (specified as anhydrous) were received from Alfa Aesar/Johnson Matthey. Ru(III)2,4-pentanedionate ($Ru(acac)_3$) and another RuO_2 material (which was not specified as being either hydrous or anhydrous) were obtained from Aldrich. All materials were used as received.

* To whom correspondence may be addressed. E-mail: rolison@nrl.navy.mil.
[†] Catholic University of America.
[‡] Naval Research Laboratory.
[§] University of Southampton.

10.1021/jp990096n CCC: $18.00
Published on Web 05/22/1999

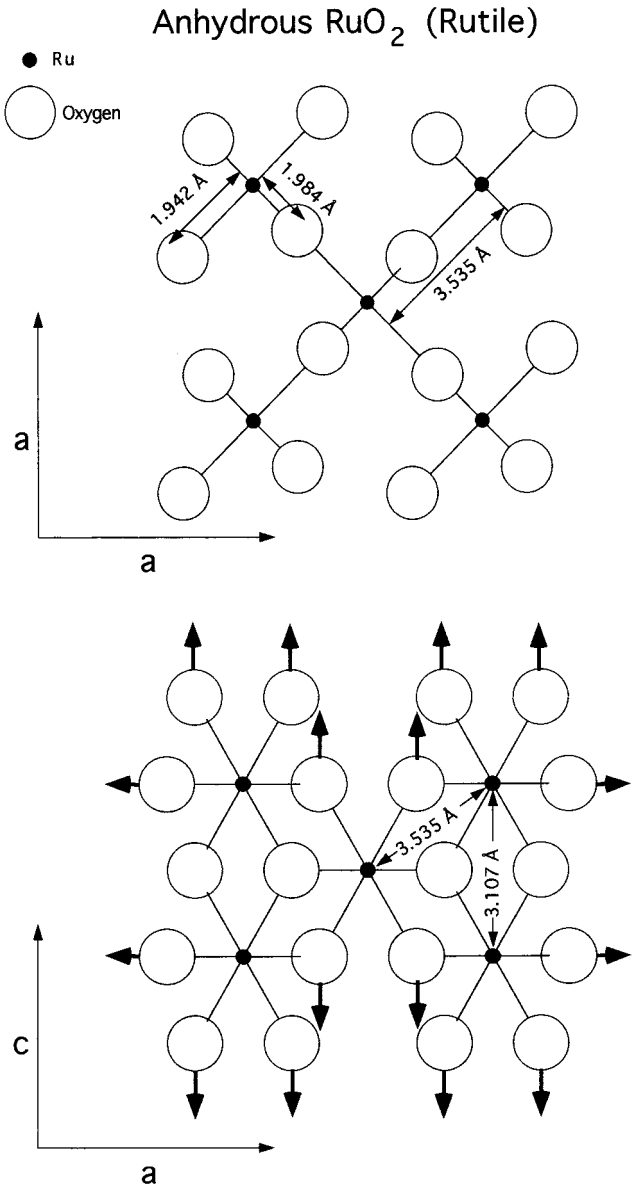

Figure 1. RuO_2 rutile crystal structure showing important Ru−O and Ru−Ru bond distances that relate to features in the RDF of anhydrous RuO_2. The top view is the *c* axis projection, and the bottom view is the *a* axis projection, where the vertical arrow pairs indicate an infinitely extending chain and the horizontal arrows indicate chains connected perpendicular to the *c* axis.

For TGA, 15−25 mg of the solid was loaded in an alumina pan and measured under flowing N_2 at 10 °C/min from 25 to 1000 °C using a TA Instruments SDT 2960 simultaneous TGA−DTA.[7,8] XRD was performed using a Rigaku model DMAX/B X-ray diffractometer operating with a rotating Cu anode at 50 kV and 40 mA.[8]

For XAS analysis of the Ru K-edge, the samples were ground with boron nitride, pressed into self-supporting pellets, and mounted in a previously described gas-treatment cell.[18] All samples were measured at room temperature in air to minimize water condensation and desorption. The measured edge jump for all samples was ~0.6, except for $Ru(acac)_3$, which had an edge jump of 1. Spectra were collected on the wiggler station 9.3 of the Synchrotron Radiation Source (SRS) at Daresbury Laboratory, UK (ring energy 2.0 GeV, ring current 110−260 mA). The Si(220) double crystal monochromator was detuned to 70% intensity to minimize the higher harmonics. The measurements were carried out in transmission mode at the Ru K-edge near 22 122 eV. The radiation intensity was measured with ion chambers optimized to the Ru K-edge.

XAS: Data Analysis. The XAS data were processed using standard procedures. The Ru K-edge steps were normalized to unity, and the data above the Ru K-edge were background subtracted to produce the $\chi(k)$ functions, where energy in electronvolts was converted to *k* space over the region from 2 to 18.0 $Å^{-1}$.[19,20] The $\chi(k)$ data were k^2-weighted and then Fourier transformed to produce a partial radial distribution function (RDF) around Ru. The $k^2\chi(k)$ data were Fourier transformed over the range 3.5 $Å^{-1} < k < 17.5$ $Å^{-1}$, using a Hanning termination window of 2.0 $Å^{-1}$ at both ends of the transform range.

The partial RDFs of the samples were analyzed using the programs FEFF (version 5.04) and FEFFIT[21−23] to obtain average bond distance (*r*), coordination number (*n*), and the Debye−Waller factor (σ^2) for each Ru−O and Ru−Ru nearest-neighbor peak. The analysis procedure was done in two steps: (1) the $\chi(k)$ function of rutile RuO_2 was calculated using FEFF, and FEFFIT was then used to fit the calculation to the experimental data for RuO_2 (anhydrous) by varying E_0 (the energy of the Ru K-edge was initially set to 0 eV), s_0^2 (an amplitude scaling factor), and σ^2, while holding the known *r* and *n* values constant (to those of the crystal structure) for each significant pair-correlation (path); and (2) the RDFs of the unknowns were fit by varying *r*, *n*, and σ^2 for each significant path by using E_0 and s_0^2 as determined from the analysis of anhydrous RuO_2. By fitting several data sets gathered for each sample, a set of *r*, *n*, and σ^2 values were determined for each sample and then averaged (see Tables 1 and 2). A range about the average or experimental error for each parameter includes all values determined from the fitting for a particular parameter.

Results and Discussion

TGA and XRD Characterization. During TGA, the Alfa $RuO_2 \cdot xH_2O$ loses 23.9% of its weight from 25 to 300 °C.[7,8] Because decomposition of RuO_2 to Ru metal should not occur at temperatures less than 1000 °C,[24] the weight loss is attributed to desorption of bound water. This weight loss corresponds to a composition of $RuO_2 \cdot 2.32H_2O$. A further 2.1 wt % loss occurs between 300 and 1000 °C under nitrogen, which may indicate formation of Ru^{3+} and loss of oxygen from the material. The RuO_2 material from Aldrich loses 3.84 wt %, indicating partial hydration and a composition of $RuO_2 \cdot 0.29H_2O$. In contrast, RuO_2 (anhydrous) loses only 0.3% of its mass over the same temperature range, presumably from desorption of surface water ($RuO_2 \cdot 0.02H_2O$). The hydrated ruthenium oxide samples will hereafter be identified by their approximate water contents.

$RuO_2 \cdot 2.32H_2O$, $RuO_2 \cdot 0.29H_2O$, and RuO_2 have markedly different XRD patterns, as would be expected for the 100-fold span in their water content. The XRD pattern for anhydrous RuO_2 has the sharp diffraction peaks expected from crystallites greater than 0.1 μm in size and matches well the pattern of rutile RuO_2.[25] The XRD profile of $RuO_2 \cdot 2.32H_2O$ has broad features,[8] indicating that it is amorphous. XRD data discussed in the literature for $RuO_2 \cdot 0.5H_2O$[8,13] indicate that peaks due to the rutile structure are not present but that removing water to form $RuO_2 \cdot 0.3H_2O$ leads to XRD-discernible rutile structure.[13]

XAS Results. *XANES.* Comparison of the Ru K-edge spectra of anhydrous RuO_2 with Ru metal (Figure 2a) shows the edge shift expected between metal and oxide that arises due to a difference in the core−hole interactions of the X-rays with the Ru^0 and Ru^{4+} in the materials.[26] The edge position of $Ru(acac)_3$, in which Ru^{3+} is coordinated only to oxygen, overlies that of anhydrous RuO_2 (see Figure 2a). Because XANES does not distinguish between Ru^{3+} and Ru^{4+}, this technique cannot be

TABLE 1: Ru EXAFS First-Shell Ru−O Fits Using the Theoretical Rutile RuO_2 Structure

sample	*r*/Å	*n*/atoms	σ^2/Å^2	χ^2
anhydrous RuO_2[a]	1.94	2.0	0.0001 ± 0.0001	18.8
	1.98	4.0	0.0057 ± 0.0001	
RuO_2·0.29H_2O (Aldrich)[b]	1.91	2.7	0.0018	3.0
	1.98	3.7	0.0048	
RuO_2·2.32H_2O (Alfa)	1.90 ± 0.01	2.5 ± 0.1	0.0145 ± 0.0012	4.1
	1.99 ± 0.01	3.9 ± 0.1	0.0068 ± 0.0005	

[a] Bond distances (*r*) and coordination numbers (*n*) listed for anhydrous RuO_2 are the actual values from the crystal structure of rutile RuO_2. [b] Only one data set was processed; therefore, no experimental errors were determined.

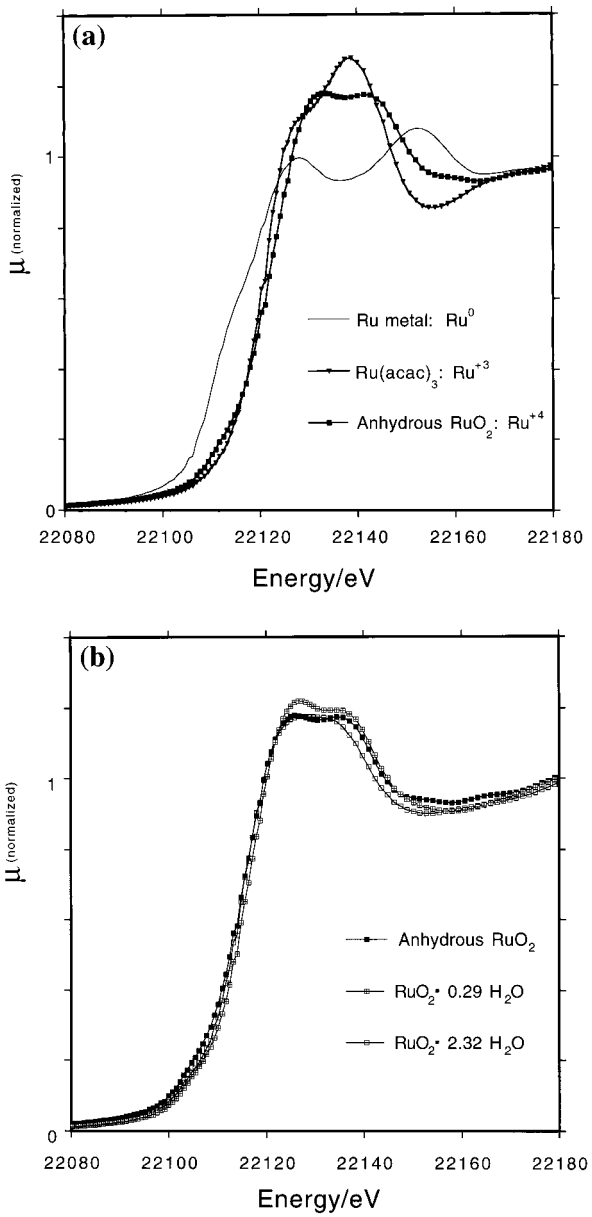

Figure 2. (a) Near-edge spectra (XANES) of Ru valence standards: Ru metal, $Ru^{III}(acac)_3$, and rutile RuO_2. (b) XANES of the Ru oxides: partially hydrous RuO_2 (RuO_2·0.29H_2O) and amorphous hydrous ruthenium oxide (RuO_2·2.32H_2O).

used to determine the fraction of Ru^{3+} in hydrous ruthenium oxide, even though Ru^{3+} centers are known to be present.[1,15,27−29] In keeping with the invariance of the K-edge for Ru(III) and Ru(IV) speciation, all three ruthenium oxide compounds exhibit no significant difference between their K-edge energies, see Figure 2b. Their near-edge features are not identical, however, which indicates that the short-range structures differ among all three of the ruthenium oxides.

TABLE 2: Ru EXAFS Second-Shell Ru−Ru Fits Using the Theoretical Rutile RuO_2 Structure

sample	*r*/Å	*n*/atoms	σ^2/Å^2	χ^2
anhydrous RuO_2[a]	3.11	2.0	0.0007 ± 0.0001	18.8
	3.54	8.0	0.0081 ± 0.0001	
RuO_2·0.29H_2O[b]	3.10	0.9	0.0008	3.0
	3.55	2.3	0.0066	
RuO_2·2.32H_2O	3.10 ± 0.01	2.1 ± 0.4	0.0030 ± 0.0007	4.1

[a] Bond distances (*r*) and coordination numbers (*n*) listed for anhydrous RuO_2 are the actual values from the crystal structure of rutile RuO_2. [b] Only one data set was processed; therefore, no experimental errors were determined.

EXAFS Analyses. Anhydrous RuO_2. In keeping with the XRD results for anhydrous RuO_2, its structure is assigned to that of rutile RuO_2. To verify this assignment, the X-ray absorption spectrum of rutile RuO_2 was calculated and used in the analysis of the EXAFS data obtained for anhydrous RuO_2. The theoretical rutile RuO_2 $\chi(k)$ was generated by using an atom cluster up to 7.0 Å from a central Ru and calculating all single scattering and multiple scattering paths in the cluster by using the program FEFF. The four largest amplitude paths from the rutile RuO_2 structure that were used to fit nearest-neighbor peaks below 4.0 Å in the RDF of RuO_2 (anhydrous) are all single scattering: Ru−O at 1.942 Å (with $n = 2$); Ru−O at 1.984 Å (with $n = 4$); Ru−Ru at 3.107 Å (with $n = 2$); Ru−Ru at 3.535 Å (with $n = 8$); see Figure 1. Contributions from Ru−O paths at distances of 3.407 and 3.664 Å, both having $n = 4$, were not included in the fitting due to their weak amplitudes.

The anhydrous RuO_2 RDF was fit over the range 1.0 Å $\leq r \leq$ 4.0 Å. All *r* and *n* values were constrained to those determined for the rutile RuO_2 structure, while varying E_0 and s_0^2 and the unknown EXAFS Debye−Waller factor for each path. The best fit was obtained with an E_0 and s_0^2 of −1.14 eV and 0.275, respectively. FEFF calculations for the rutile RuO_2 structure overestimated the EXAFS amplitude by a factor of 2−3 with respect to the anhydrous RuO_2 data; this overestimate resulted in a smaller s_0^2 value from the fitting. Debye−Waller factors determined for each path are listed in Tables 1 and 2. The quality of the fit and the reasonable values of the parameters obtained from the fitting indicate that the structure of anhydrous RuO_2 can be considered to be rutile RuO_2 and suitable as a standard for the other two Ru oxides investigated here.

The theoretical RDF includes the basic features of the nearest-neighbor peaks below 4 Å in the RDF of anhydrous RuO_2 (Figure 3a). The theoretical $\chi(k)$ function overlies many of the major features in the $\chi(k)$ data of anhydrous RuO_2 (Figure 3b), but several features are missing in the theoretical RDF because the calculation does not include contributions from the 4.2 Å and 5.2 Å peaks in the experimental RDF (Figure 3a). The theory does not fit either the experimental amplitude of the Ru−Ru peaks at 2.8 and 3.2 Å in the RDF or the nearest-neighbor Ru−O peak at 1.6 Å. These errors are due to interference effects between the 3.11 Å and 3.54 Å Ru−Ru contributions in the

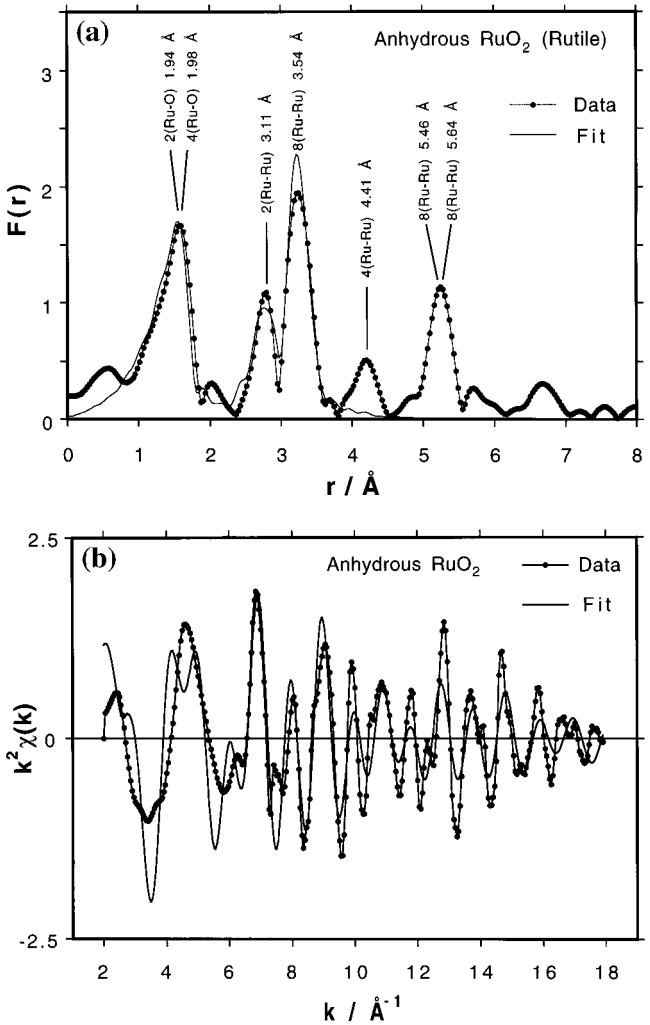

Figure 3. (a) Anhydrous RuO_2 partial RDF data (points and line) and fit (line only) done by FEFFIT using the RuO_2 rutile structure. (b) $k^2\chi(k)$ data and fit. Pair correlation bond distances and coordination numbers for the first five peaks in the RDF are shown.

$k^2\chi(k)$ data, which can strongly affect the amplitudes and widths of these two peaks in the RDF.

Hydrous Ruthenium Oxides. To fit the RDFs of the two hydrous ruthenium oxides, the rutile RuO_2 paths outlined above were used. The values for r, n, and σ_0^2 were varied for each path, while the E_0 and s_0^2 values determined from the analysis of anhydrous RuO_2 were held constant. Comparing the RDF of $RuO_2 \cdot 0.29H_2O$ to that of anhydrous RuO_2 (Figure 4a) shows that both have similar nearest-neighbor octahedral environments but exhibit significant differences for the longer range Ru−Ru correlations. Fitting the major features below 4.0 Å in the partial RDF for $RuO_2 \cdot 0.29H_2O$ (parts b and c of Figure 4) required using all four paths from the theoretical RuO_2 rutile structure. The first-shell Ru−O parameters for $RuO_2 \cdot 0.29H_2O$ are similar to those determined for anhydrous RuO_2 (Table 1). The amplitude of the second shell peaks for $RuO_2 \cdot 0.29H_2O$ are considerably damped compared with the second-shell Ru−Ru peaks for anhydrous RuO_2, which is reflected in the smaller n values obtained in the fitting for the $RuO_2 \cdot 0.29H_2O$ data (Table 2).

The RDFs of anhydrous RuO_2 and amorphous $RuO_2 \cdot 2.32H_2O$ are compared in Figure 5a. The amorphous sample has no structural correlations beyond the Ru−Ru peak at 2.8 Å, indicating that $RuO_2 \cdot 2.32H_2O$ is greatly disordered, even at the level of local structure. To fit the major features below 4.0 Å

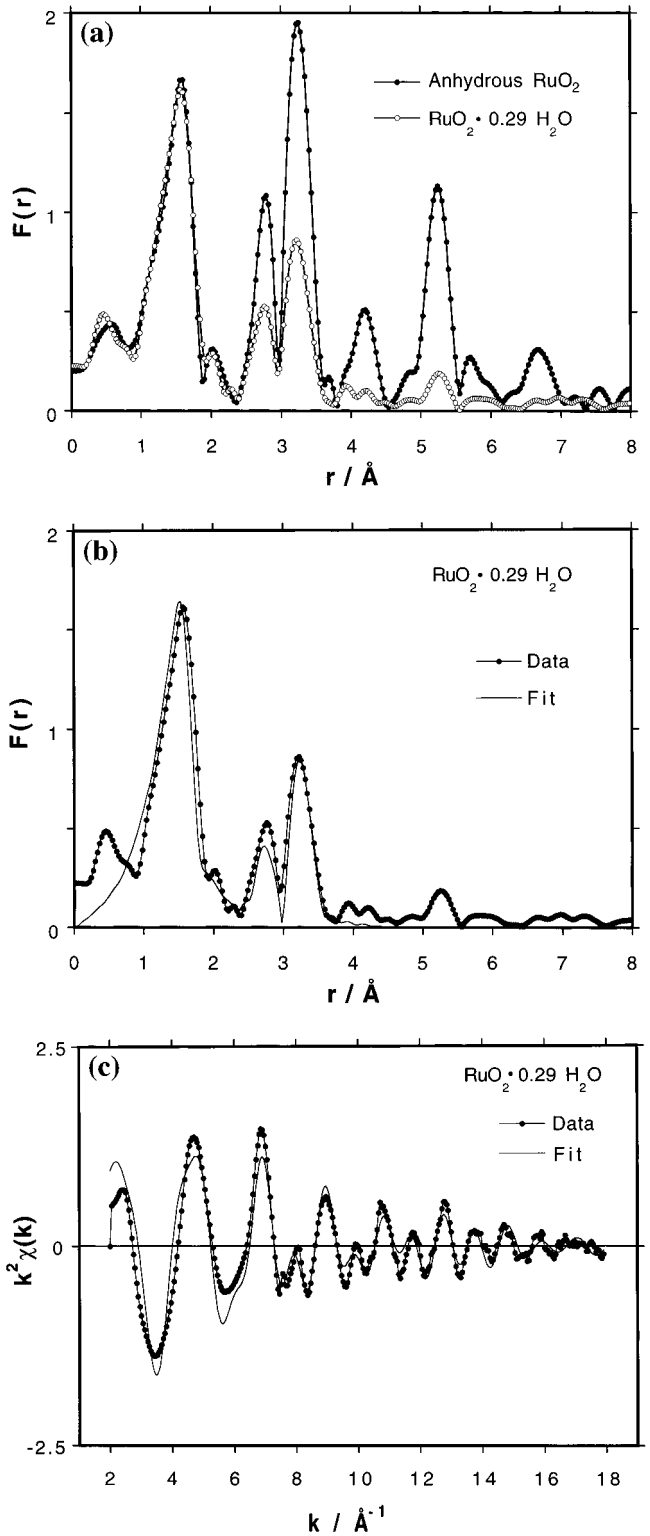

Figure 4. (a) RDF comparison of anhydrous RuO_2 and $RuO_2 \cdot 0.29H_2O$. (b and c) $RuO_2 \cdot 0.29H_2O$: partial RDF data and fit, and $k^2\chi(k)$ data and fit.

in the partial RDF required contributions from three of the four paths from the theoretical RuO_2 rutile structure (parts b and c of Figure 5). The fitting results show that the two Ru−O and single Ru−Ru pair correlations from the first and second shells in the amorphous sample are considerably more disordered than those in anhydrous RuO_2, as seen by the large Debye−Waller factors determined for $RuO_2 \cdot 2.32H_2O$ (Tables 1 and 2).

The small, narrow peak near 2.2 Å in the RDF of $RuO_2 \cdot 2.32H_2O$ cannot be fit using the paths from the rutile RuO_2

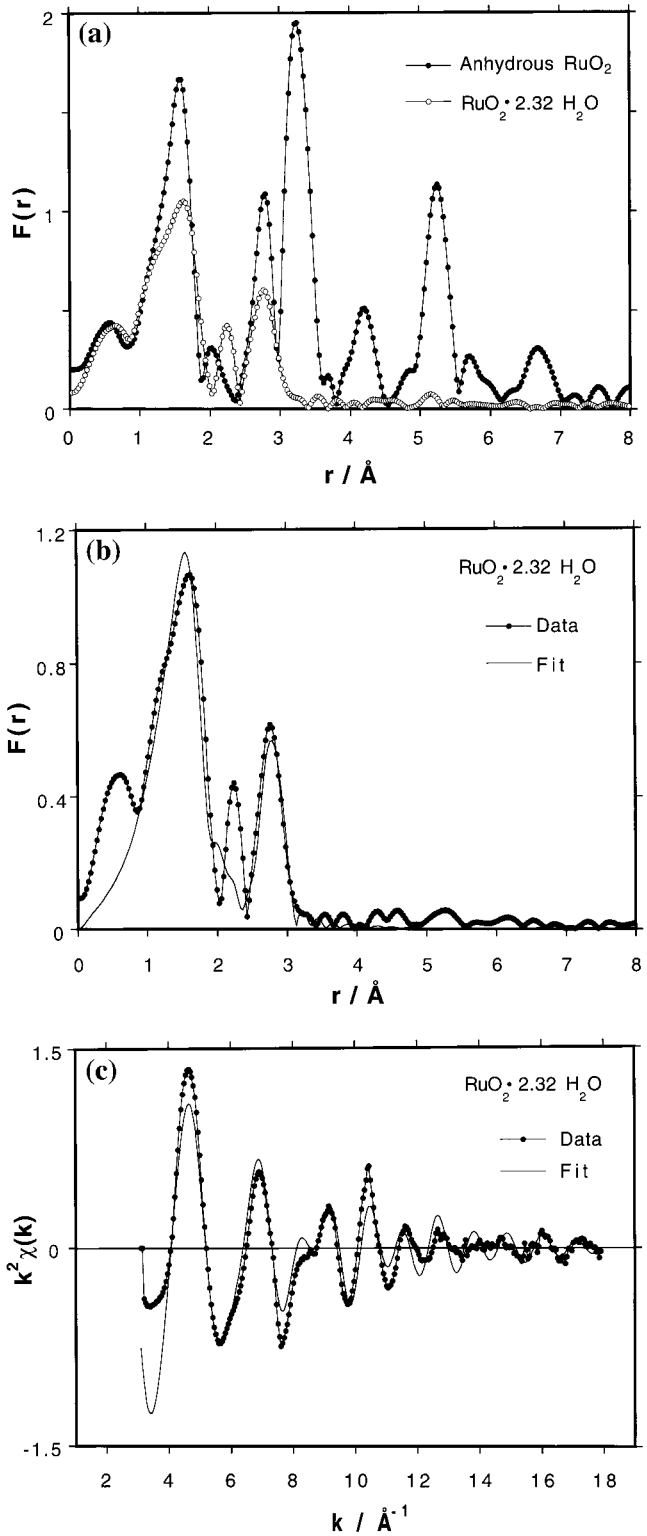

Figure 5. (a) RDF comparison of anhydrous RuO_2 and amorphous $RuO_2 \cdot 2.32H_2O$. (b and c) $RuO_2 \cdot 2.32H_2O$: partial RDF data and fit, and $k^2\chi(k)$ data and fit.

structure (Figure 5b). To determine if this peak is a real structural feature or an artifact from the Fourier transform, the $k^2\chi(k)$ generated from the fit was compared with the $k^2\chi(k)$ data (Figure 5c). The fit describes most of the features in the data except for amplitude discrepancies at 10 Å$^{-1} < k < 15$ Å^{-1}. The $k^2\chi(k)$ generated from the fit was then subtracted from the $k^2\chi(k)$ data to produce a difference $\chi(k)$ function that has oscillations from 10 to 15 Å^{-1}. The Fourier transform of this difference function is dominated by the 2.2 Å peak, which indicates that this peak is due to the absence of oscillation amplitude in the 10−15 Å^{-1} range in the $k^2\chi(k)$ data. An absence of oscillation amplitude within part of the $\chi(k)$ data can be caused by two components having similar, but different frequencies or a beat phenomenon; the two frequency components in this case are the peaks near 2.2 and 2.75 Å in the RDF of $RuO_2 \cdot 2.32H_2O$. Since all three $k^2\chi(k)$ data sets analyzed for $RuO_2 \cdot 2.32H_2O$ have this absence of EXAFS amplitude, the 2.2 Å peak appears to be due to a real structural feature and not due to an artifact of the analysis.

Structure of Hydrous Ruthenium Oxides. Comparison of the RDFs in Figure 4a and the fitting results in Tables 1 and 2 indicate that $RuO_2 \cdot 0.29H_2O$ has RuO_6 octahedra characteristic of rutile RuO_2. The RDFs of $RuO_2 \cdot 0.29H_2O$ and anhydrous RuO_2 differ primarily in that $RuO_2 \cdot 0.29H_2O$ has considerably smaller amplitude Ru−Ru correlations. This difference indicates that discrepancies exist between the structure of the hydrous and anhydrous materials beyond the first coordination shell of the Ru.

Two different structures can be interpreted from the EXAFS data for $RuO_2 \cdot 0.29H_2O$. The first structural interpretation explicitly accepts the bond distances and coordination numbers in Table 2. This condition requires that fewer nearest-neighbor Ru atoms surround each Ru in $RuO_2 \cdot 0.29H_2O$ (than in rutile RuO_2) so that each RuO_6 octahedron can only be linked to one other octahedron. These octahedral "dimers" must share oxygens (on average) with two other dimers to explain the 3.55 Å pair correlation with $n = 2.3$ (Figure 6a).

A more likely interpretation of the structural parameters in Table 2 posits an ordered core (i.e., the rutile RuO_6 octahedron) surrounded by a progressively less ordered rutile structure. This interpretation can be justified by RDF features in Figure 4a, where very weak peaks for $RuO_2 \cdot 0.29H_2O$ correspond with Ru−Ru peaks out to 6 Å in the RDF of anhydrous RuO_2. Debye−Waller factors and coordination numbers are correlated variables in EXAFS analysis, so the reduction in coordination number may also be explained as being due to increased structural disorder. In the disordered model, the octahedral chains can be twisted or distorted with respect to those in the rutile structure, to create a range of Ru−Ru distances in the structure. At distances beyond the 3.54 Å Ru−Ru correlation, this partially hydrated phase appears to be almost completely disordered to the point where there is little structural similarity between this phase and rutile RuO_2.

The EXAFS amplitude of $RuO_2 \cdot 2.32H_2O$ is more damped than that of $RuO_2 \cdot 0.29H_2O$ (compare Figures 5a and 4a). The damping implies significant disorder in the first coordination shell around the Ru, indicating that its RuO_6 octahedra are more disordered than in anhydrous RuO_2 or $RuO_2 \cdot 0.29H_2O$. The absence of the 3.54 Å Ru−Ru peak in the RDF of this amorphous hydrous phase (Figure 5b) indicates that no three-dimensional networks of linked RuO_6 octahedral chains exist in $RuO_2 \cdot 2.32H_2O$. The 3.10 Å Ru−Ru peak has a considerably larger Debye−Waller factor than those determined for anhydrous RuO_2 and $RuO_2 \cdot 0.29H_2O$ indicating that there are disordered octahedral chains in this structure, as depicted in Figure 6b.

The unexplained 2.2 Å peak in the RDF of the amorphous phase ($RuO_2 \cdot 2.32H_2O$) may be due to a structural pair correlation. On the basis of the typical phase shifts of peaks in the Ru RDFs with respect to their actual bond distances, this peak would correspond to a bond distance ranging from ∼2.44 to 2.61 Å. Assigning the 2.2 Å peak to Ru−OH or Ru−OH_2 pair correlations would be logical for a hydrous material, but a bond

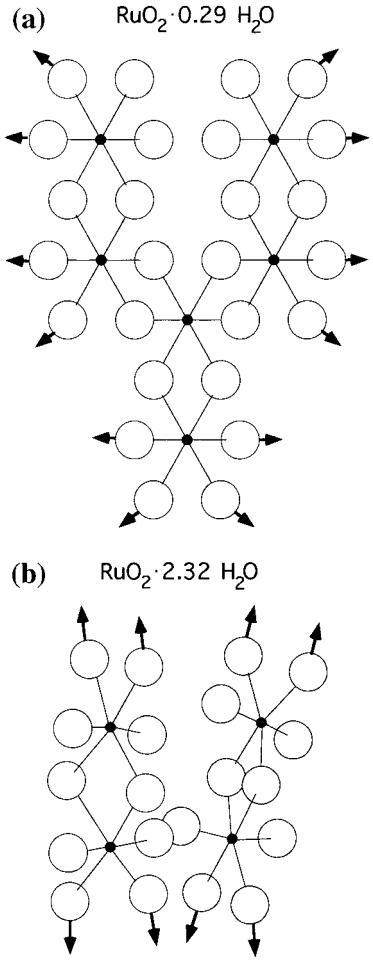

Figure 6. (a) Hypothetical fragment of the $RuO_2 \cdot 0.29H_2O$ structure from EXAFS analysis results featuring RuO_6 octahedral dimers, where each octahedron is linked to two other dimers. (b) Hypothetical fragment of the amorphous $RuO_2 \cdot 2.32H_2O$ structure from EXAFS analysis results featuring disordered RuO_6 octahedra linked in twisted, unconnected chains; arrows indicate infinitely extending chains.

length greater than 2.4 Å cannot be reconciled with known Ru−OH or Ru−OH_2 bonds in the solid state. Crystalline tosylate salts of $Ru(OH_2)_6^{2+}$ and $Ru(OH_2)_6^{3+}$ have Ru−OH_2 bond lengths of 2.122 and 2.029 Å, respectively,[30] while the Ru−OH distance in $Ba[Ru^{VI}(O)_3(OH)_2]$[30] is 2.02 Å. A possible explanation for the 2.2 Å peak is that the hydrated oligomers implicit in the local structure of $RuO_2 \cdot 2.32H_2O$ (>four water molecules for every Ru−Ru dimer) yield longer Ru−OH or Ru−OH_2 bonds than found in crystalline compounds because of hydrogen bonding in this solution-like structure.

Correlation between Local Structure of $RuO_2 \cdot xH_2O$ and its Charge Storage Properties. The high specific capacitance of hydrous ruthenium oxides results from a pseudocapacitive effect whereby both protons and electrons are "double injected" from an acidic electrolyte into the surface of hydrous ruthenium oxide, as described in eq 1.[3,27−29]

$$RuO_x(OH)_y + \delta H^+ + \delta e^- \leftrightarrow RuO_{x-\delta}(OH)_{y+\delta} \qquad (1)$$

Although it is not apparent from eq 1, the Ru^{4+} cation is reduced while the oxygen ion in its site is protonated. To conserve charge and site balance, the full electron/proton reaction is written as[31]

$$Ru^{IV}-O^{2-} + H^+ + e^- \leftrightarrow Ru^{III}-OH^- \qquad (2)$$

Charge is stored and discharged with the concomitant exchange of protons and electrons from the mixed-conducting material. The capacitance of RuO_xH_y has been correlated to several variables, including surface area, water content, electronic conductivity, and crystallinity.[13,14,16,29,31]

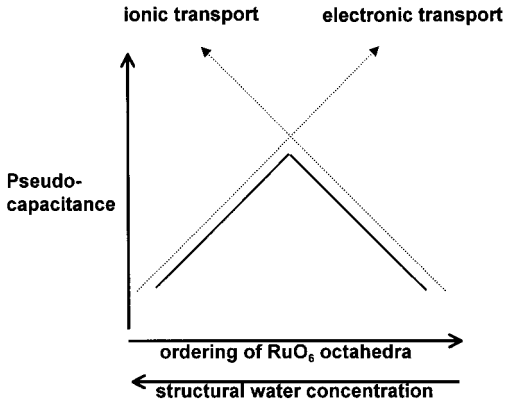

Figure 7. Schematic diagram of the trends of electron transport and proton transport in an ideal mixed conducting oxide structure.

In a system such as a pseudocapacitor, in which both electrons and cations have to be transported, facile transport paths for both types of charge carriers must exist.[32] However, structures that promote transport of one class of charge carrier do not in general promote the other. In high-temperature mixed-conducting oxides, in which electrons and oxygen-ion vacancies transport,[33] electrocatalytic efficacy should be maximized when the transport numbers for each type of charge carrier are equal. Analogously, pseudocapacitance should be optimized when the transport of electrons and protons in the structures are balanced, as shown schematically in Figure 7 for an ideal mixed conductor.

The specific capacitance obtained for hydrous ruthenium oxides[8,13] as a function of water content in the structure (which is a function of annealing temperature) is plotted in Figure 8. The amount of charge stored in the material is not a monotonic function of water content; a maximum occurs as expected for a mixed conductor and as generally shown in Figure 7. Unannealed hydrous ruthenium oxide, with at least two water molecules per RuO_2, has a specific capacitance of 527 F/g.[13] The specific capacitance reaches a maximum of 720 F/g[13] to 900 F/g[8] after it is annealed at 150 °C and has the approximate formula of $RuO_2 \cdot 0.5H_2O$. When annealed at temperatures over 150 °C, the capacitance of the hydrous ruthenium oxide decreases coincident with the appearance of rutile RuO_2 peaks in the X-ray powder diffraction pattern.[8,13] Partially hydrated ruthenium oxides, having formulas near $RuO_2 \cdot 0.3H_2O$, have specific capacitances of ~600 F/g. The specific capacitance of hydrous ruthenium oxides that have been dehydrated at 400 °C to $RuO_2 \cdot 0.03H_2O$ is 19 F/g[13] to 29 F/g,[8] indicating that the water is structural and involved in proton transport. In contrast, RuO_2 that is derived from anhydrous preparations (and which has only physisorbed water) has a specific capacitance of 0.75 F/g,[8] so it is not a charge storage material.

The EXAFS-derived local structures of $RuO_2 \cdot 2.32H_2O$, $RuO_2 \cdot 0.29H_2O$, and rutile RuO_2 are also shown in Figure 8 for comparison to their position on the specific capacitance curve. Although $RuO_2 \cdot 2.32H_2O$ is amorphous by X-ray diffraction, it still maintains disordered oligomers of RuO_6 octahedra. These octahedra become progressively more ordered and connected as the water content of the RuO_xH_y decreases, and the material begins to exhibit XRD-discernible rutile RuO_2 structure. As the RuO_6 octahedra become more three dimensionally ordered, the electronic conductivity of the ruthenium oxide increases, e.g., electronic conductivity of single-crystal RuO_2 (10^4 S cm)[34] >

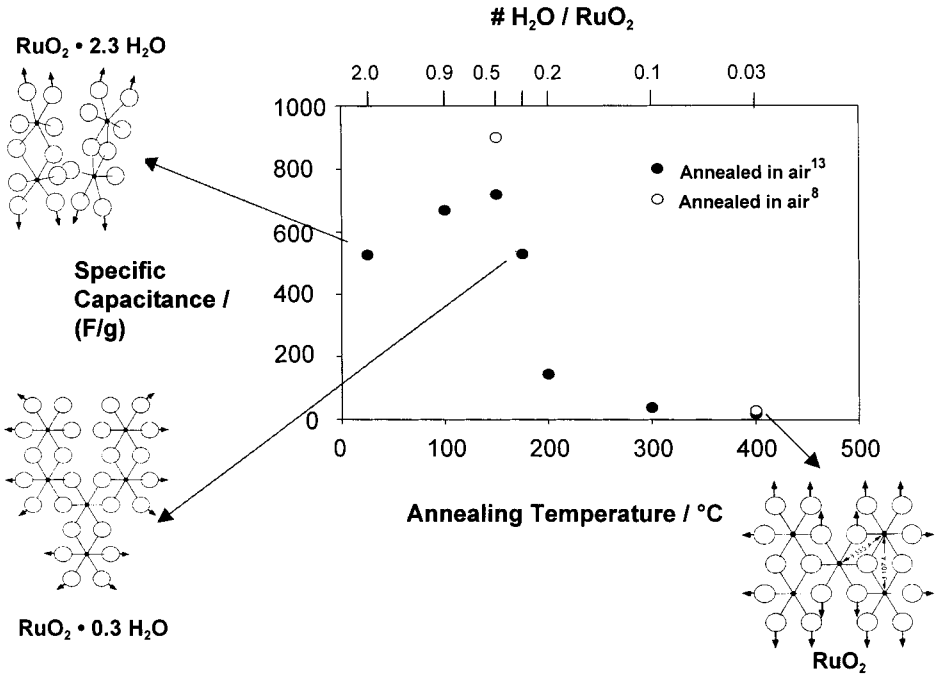

Figure 8. Specific capacitance of various $RuO_2 \cdot xH_2O$ solids as a function of annealing temperature and number of water molecules per RuO_2; the EXAFS-derived local structures that exist at various points on the specific capacitance curve are shown as insets. The specific capacitance was determined in 1 M H_2SO_4 electrolyte.

polycrystalline RuO_2 ($\sim 10^3$ S cm)[35] > hydrous ruthenium oxide ($\sim$1 S cm).[36] Magnetic susceptibility measurements show that a similar electron conduction mechanism along dioxo bridges occurs for RuO_2 whether amorphous, defective, or anhydrous.[36]

Even with the limited set of related RuO_xH_y solids described in this study, two vastly different structures share the same physical property: they store the same amount of electrical charge. The disrupted, nearly solution-like local structure obtained for $RuO_2 \cdot 2.32H_2O$ has a specific capacitance comparable to that for $RuO_2 \cdot 0.29H_2O$, which has a local structure consisting of rutile RuO_6 octahedra interconnected in chains but without extended order. When opposing trends in transport exist, as depicted in Figure 7, materials of differing composition and local structure can express the same specific capacitance because they balance the competing electron/proton transport requirements but do so on either side of the maximum specific capacitance. From the EXAFS-derived structures and the known specific capacitances, we can infer that for optimum charge storage in these mixed conductors, the local structure requires both more interconnected RuO_6 octahedra than found in $RuO_2 \cdot 2.32H_2O$ and more structural water than in $RuO_2 \cdot 0.29H_2O$.

Conclusions

Ru EXAFS data were collected and analyzed for the crystalline standard, rutile RuO_2, and for the unknown structure phases, partially hydrated RuO_2 ($RuO_2 \cdot 0.29H_2O$) and hydrous $RuO_2 \cdot 2.32H_2O$. Analysis results for $RuO_2 \cdot 0.29H_2O$ indicate that the structure is a disordered RuO_2 rutile-like structure, where the RuO_6 octahedra are similar to those found in the crystal structure, while the three-dimensional network of octahedral chains does not extend as far as that in RuO_2 rutile. Amorphous $RuO_2 \cdot 2.32H_2O$ has disordered RuO_6 octahedra connected in chains, but the data show no evidence of a three-dimensional network of octahedra. The orientation of water within this structure is not discernible from the EXAFS data, but clearly the presence of structural water disrupts the three-dimensional rutile structure.

The structures of RuO_xH_y materials correlate to their mixed conductivity and pseudocapacitance. The local structures of RuO_xH_y materials control their electrical properties by how they balance electron and proton transport. Charge storage in RuO_xH_y materials is maximized when the local structures retain facile transport pathways for both electrons and protons. Other than in glasses, one does not normally consider engineering amorphous structure to maximize a physical property, but in the case of pseudocapacitive materials, control of the amorphous structure is paramount.

Acknowledgment. This work was supported by DARPA (the Defense Advanced Research Projects Agency), ONR (U.S. Office of Naval Research), and the CLRC (Central Laboratory of the Research Councils, UK). The authors wish to thank Daresbury Laboratory for the allocation of beamtime, Prof. D. C. Koningsberger for the loan of the gas-treatment cell, R. J. Mathew and R. A. Lampitt for assistance with the data collection, C. I. Merzbacher (NRL) for support of the data analyses, and R. G. Nuzzo and A. I. Frenkel (University of Illinois-Urbana−Champaign) for helpful comments. K.E.S. acknowledges an ASEE-NRL Postdoctoral Research Associateship, 1993−1996.

References and Notes

(1) Swider, K. E.; Merzbacher, C. I.; Hagans, P. L.; Rolison, D. R. *Chem. Mater*. **1997**, *9*, 1248.

(2) Goodenough, J. B. *Prog. Solid State Chem*. **1971**, *5*, 145.

(3) Trasatti, S. *Electrochim. Acta* **1991**, *36*, 225 and references therein.

(4) Trasatti, S.; O'Grady, W. E. In *Advances in Electrochemistry and Electrochemical Engineering*; Gerischer, H., Tobias, C., Eds.; J. Wiley: New York, 1981; Vol. 12, pp 177−261.

(5) Battaglin, G.; Carnera, A.; Della Mia, G. *J. Chem. Soc., Faraday Trans.* **1985**, *81*, 2995.

(6) Trasatti, S.; Lodi, G. In *Electrodes of Conductive Metallic Oxides*; Trasatti, S., Ed.; Elsevier: Amsterdam, 1981; Part B, Chapter 10.

(7) Hagans, P. L.; Swider, K. E.; Rolison, D. R. In *Electrode Materials and Processes for Energy Conversion and Storage IV*; McBreen, J., Srinivasan, S., Eds.; PV 97−13; Electrochemical Society: Pennington, NJ, 1997; pp 86−105.

(8) Rolison, D. R.; Hagans, P. L.; Swider, K. E.; Long, J. W. *Langmuir* **1999**, *15*, 774.

(9) Long, J. W.; Rolison, D. R. In *New Directions in Electroanalytical Chemistry*; Leddy, J., Porter, M. D., Vanysek, P., Eds.; PV 99−5; The Electrochemical Society: Pennington, NJ, 1999; pp 125−131.
(10) Rolison, D. R.; Hagans, P. L.; Swider, K. E.; Long, J. W. Disclosure of Invention, Naval Research Laboratory, Navy Case 79,315, June 1998.
(11) Trojanek, A.; Kalvoda, R. *Trans. SAEST* **1977**, *12*, 45.
(12) Mills, A.; Lawrence, C.; Enos, R. *J. Chem. Soc., Chem. Commun.* **1984**, 1436.
(13) Zheng, J. P.; Cygan, P. J.; Jow, T. R. *J. Electrochem. Soc.* **1995**, *142*, 2699.
(14) Jow, T. R.; Zheng, J. P. *J. Electrochem. Soc.* **1998**, *145*, 49.
(15) Swider, K. E.; Merzbacher, C. I.; Hagans, P. L.; Rolison, D. R. *J. Non-Cryst. Solids* **1998**, *225*, 348.
(16) Long, J. W.; Swider, K. E.; Merzbacher, C. I.; Rolison, D. R. *Langmuir* **1999**, *15*, 780.
(17) Triggs, P. *Helv. Phys. Acta* **1985**, *58*, 657.
(18) Kampers, F. W. H.; Maas, T. M. J.; van Grondelle, J.; Brinkgreve, P.; Koningsberger, D. C. *Rev. Sci. Instrum.* **1998**, *60*, 2635.
(19) The energy in electronvolts was converted to k in $Å^{-1}$.[20]
(20) Sayers, D. E.; Bunker, B. A. In *X-ray Absorption, Principles, Applications, Techniques of EXAFS, SEXAFS, and XANES*; Koningsberger, D. C., Prins, R., Eds.; J. Wiley: New York, 1988; p 211.
(21) Rehr, J. J.; Albers, R. C.; Mustre de Leon, J. *Physica B* **1989**, *158*, 417.
(22) Rehr, J. J.; Mustre de Leon, J.; Zabinsky, S. I.; Albers, R. C. *J. Am. Chem. Soc.* **1991**, *113*, 5135.
(23) Mustre de Leon, J.; Rehr, J. J.; Zabinsky, S. I.; Albers, R. C. *Phys. Rev. B* **1991**, *44*, 4146.
(24) Campbell, P. F.; Ortner, M. H.; Anderson, C. J. *Anal. Chem.* **1961**, *33*, 58.
(25) JCPDS-ICDD #43−1027.
(26) Bhide, V. G.; Kaicker, S. K. *J. Phys. Chem. Solids* **1974**, *35*, 695.
(27) Trasatti, S. *Platinum Met. Rev.* **1994**, *38*, 46.
(28) Rishpon, J.; Gottesfeld, S. *J. Electrochem. Soc.* **1984**, *131*, 1961.
(29) Sarangapani, S.; Tilak, B. V.; Chen, C.-P. *J. Electrochem. Soc.* **1996**, *132*, 3791.
(30) Wilkinson, G., Gillard, R. D., McCleverty, J. A., Eds. *Comprehensive Coordination Chemistry*; Pergamon: Oxford, 1987; Vol. 4, pp 420−423.
(31) Yamada, A.; Goodenough, J. B. *J. Electrochem. Soc.* **1998**, *145*, 737.
(32) Huggins, R. A. *Ionics* **1997**, *3*, 379.
(33) Tuller, H. L. In *Non-Stoichiometric Oxides*; Sorenson, O. T., Ed.; Academic Press: New York, 1981; p 271.
(34) Schafer, H.; Schneidereit, G.; Gerhardt, W. *Z. Anorg. Allg. Chem.* **1963**, *319*, 372.
(35) Krusin-Elbaum, L. *Thin Solid Films* **1989**, *169*, 17.
(36) Fletcher, J. M.; Gardner, W. E.; Greenfield, B. F.; Holdoway, M. J.; Rand, M. H. *J. Chem. Soc. A* **1968**, 653.